



NLR-TP-2013-107

## **Fatigue crack growth in highly loaded components**

R.A. Huls, F.P. Grooteman and R.P.G. Veul

**Nationaal Lucht- en Ruimtevaartlaboratorium**

National Aerospace Laboratory NLR

Anthony Fokkerweg 2

P.O. Box 90502

1006 BM Amsterdam

The Netherlands

Telephone +31 (0)88 511 31 13

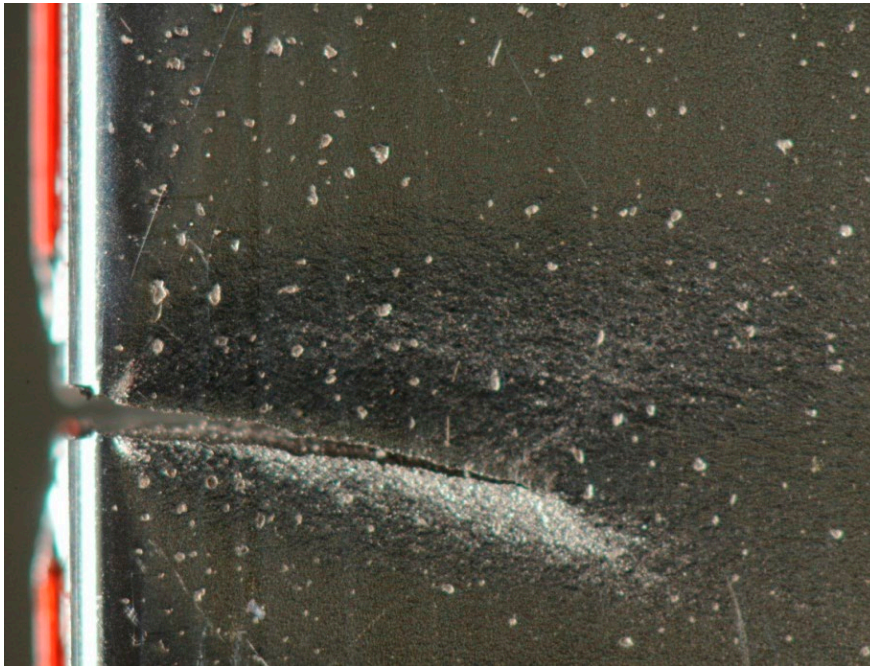
Fax +31 (0)88 511 32 10

Web site: <http://www.nlr.nl>



## Executive summary

# Fatigue crack growth in highly loaded components

**Report no.**

NLR-TP-2013-107

**Author(s)**

R.A. Huls  
F.P. Grooteman  
R.P.G. Veul

**Report classification**

UNCLASSIFIED

**Date**

July 2013

**Knowledge area(s)**

Levensduurbewaking en  
onderhoud van vliegtuigen

**Descriptor(s)**

fracture mechanics  
crack growth  
LEFM  
EPFM

**Problem area**

The current design approach for highly loaded components experiencing widespread plastic deformation is based on a classic damage tolerance approach consisting of a crack growth analysis in which the time is computed to grow an initial crack to a critical size. This can lead to both an over conservative as well as a non-conservative design.

**Description of work**

Fatigue crack growth tests were performed on IN718 with and without plastic pre-deformation.

Tests were also performed under high fatigue loads using both constant amplitude and variable amplitude loading. A model was developed to predict the fatigue crack growth for highly loaded launcher components.

**Results and conclusions**

Plastic pre-deformation did not have a significant influence on the measured growth rates and Linear Elastic Fracture Mechanics (LEFM) models remain applicable. Fatigue crack growth rates under high fatigue loads deviate significantly from the conventional LEFM data

from NASGRO database. The rates show Paris like behaviour up to the fracture toughness found in the literature. When these data are used, LEFM can be used to predict fatigue crack growth rates.

**Applicability**

The developed fatigue crack growth rate models can be applied to predict fatigue crack growth rates for highly loaded launcher components.



NLR-TP-2013-107

## Fatigue crack growth in highly loaded components

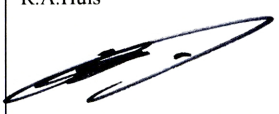
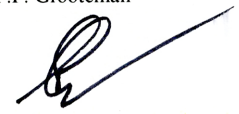

R.A. Huls, F.P. Grooteman and R.P.G. Veul

This report is based on a presentation held at the 27th Symposium of the International Conference on Aeronautical Fatigue (ICAF), Jerusalem, Israel, June 5-7, 2013.

The contents of this report may be cited on condition that full credit is given to NLR and the authors. This publication has been refereed by the Advisory Committee AEROSPACE VEHICLES.

Customer European Space Agency  
Contract number 4000102474/11/NL/RA  
Owner European Space Agency  
Division NLR Aerospace Vehicles  
Distribution Unlimited  
Classification of title Unclassified  
July 2013

Approved by:

Author R.A.Huls 	Reviewer F.P. Grooteman 	Managing department A.M. Vollebregt 
Date: 3-5-2013	Date: 6-5-2013	Date: 13/5/13



## Summary

The current design approach for highly loaded components experiencing widespread plastic deformation is based on a classic damage tolerance approach consisting of a crack growth analysis in which the time is computed to grow an initial crack to a critical size. This can lead to both an over conservative as well as a non-conservative design. Fatigue crack growth tests were performed on IN718 with and without plastic pre-deformation. Tests were also performed under high fatigue loads using both constant amplitude and variable amplitude loading. Plastic pre-deformation did not have a significant influence on the measured growth rates and LEFM models remain applicable. Fatigue crack growth rates under high fatigue loads deviate significantly from the conventional LEFM data from NASGRO database. The rates show Paris like behaviour up to the fracture toughness found in the literature. When these data are used, LEFM can be used to predict fatigue crack growth rates.

## **Contents**

<b>1</b>	<b>Introduction</b>	<b>5</b>
<b>2</b>	<b>Experimental programme</b>	<b>6</b>
<b>3</b>	<b>Analysis</b>	<b>17</b>
<b>4</b>	<b>Conclusions</b>	<b>23</b>
	<b>References</b>	<b>24</b>



## 1 Introduction

Launcher structures often contain components that undergo widespread plastic deformation due to the high loads in their relatively short operating life. The current design approach for such highly loaded components is based on a classic damage tolerance approach consisting of an LEFM crack growth analysis in which the time is computed to grow an initial crack to a critical size. Load interaction effects are generally not taken into account. It is unclear whether the linear elastic fracture mechanics (LEFM) methodology can still be applied at these high load levels. Furthermore, the non-interaction methodology can result in an over-conservative design or in particular cases even an unsafe design due to crack acceleration, depending on the nature of the variable amplitude load spectrum. To examine these issues, ESA started the technology research programme (TRP) “Fracture control/Damage tolerance methods for highly loaded launcher components”.

The main objective of this ESA TRP project was to examine the benefits of more advanced damage tolerance approaches for the prediction of highly loaded structural launcher components than the classic damage tolerance approach. The study examined application of load interaction models, but also included probabilistic methods and other new methodologies for these types of structures. The results of the load interaction part will be presented in this paper. The two important questions considered are whether linear elastic fracture mechanics (LEFM) can still be applied for these highly loaded structures and which, if any, retardation model should be used for these structures.

To answer these two questions, an experimental campaign was set up to create a data set to validate models against. A basic set of constant amplitude (CA) fatigue crack growth tests was performed on IN718 MT specimens under conventional LEFM loads. The same tests were performed on test samples that had seen an additional plastic deformation before creating the starter notch to evaluate the effect of plastic deformation on the fatigue crack growth rates. Constant amplitude displacement controlled tests were then performed on single edge crack tension specimens to evaluate the behaviour at high loads as opposed to the conventional LEFM loads applied to the MT specimens. Finally, tests were performed for variable amplitude displacement controlled loads to evaluate retardation effects.

The results of the fatigue crack growth tests are processed into fatigue crack growth rate versus stress intensity factor ranges based on LEFM and compared to calculated fatigue crack growth data. The data are also compared with the test data contained in NASGRO [1]. A fatigue crack growth model is developed based on the data from the CA tests and this model is used to predict the variable amplitude data to evaluate whether a retardation model is useful for these structures.

## 2 Experimental programme

### Material

The material selected is the nickel based superalloy Inconel 718, delivered according to the AMS 5596J standard in a sheet of 1000 x 915 x 3.18 mm. Inconel 718 is a widely applied material for engine and launcher components. Furthermore the material availability is reasonable and reference data is readily available in the NASGRO database against which the current experimental results can be compared. The heat treatment performed follows the prEN2407 standard [2], which is a conventional heat treatment (CHT). The temperature profile was recorded for verification of the proper heat treatment. Hardness measurements on various locations of two specimens per run were performed yielding values within the expected range. All the specimens were made from the same sheet of material.

### Test matrix

An overview of the test matrix is depicted in Table I. Static and fatigue crack growth tests were performed at room temperature to exclude additional uncertainty caused by fatigue crack growth under high temperature. Static tests were performed to obtain static material properties and to verify material quality. Load controlled fatigue crack growth tests on middle crack tension (MT) specimens at 10 Hz were performed to determine the fatigue crack growth rate in the standard condition as well as after application of a 1.3% total pre-strain. The MT crack growth data served as reference for the single edge crack tension (SET) tests. The large scale plasticity tests were performed on SET specimens under displacement control. Displacement control was used to avoid breaking the specimens when loading close to the yield limit. It is also an important load condition caused by the differences in thermal expansion in launcher structures. Tests were performed for constant amplitude as well as for a typical variable amplitude (VA) engine spectrum close to the yield stress and with a reduced mean. The higher loads required a decrease in test frequency and 1 Hz was chosen for the constant amplitude tests. The variable amplitude tests were performed at 2 Hz to decrease test time while maintaining correct load application. Additional SET tests were performed at a four times lower test frequency showing severe static crack growth yielding a much lower life and thus indicating a significant frequency influence.

Test type	Nr. of spec.	Test Id	Test freq. (Hz)
Static tests on ASTM E-8M specimens			
L-direction	3	L	-
T-direction	3	T	-
Moderate load fatigue crack growth tests on MT specimens			
Elastic	4*1	CA-LS3a	10
Plastic (1.3%)	4*1	CA-LS3b	10
Large scale plasticity fatigue crack growth tests on SET specimens			
Around yield stress	2	CA-LS1a	1
	2	VA-LS1b	2
With relaxed mean	2	CA-LS2a	1
	2	VA-LS2b	2

Table I: Test matrix

#### Static tests

To determine the static material properties in both directions, standard static specimens according to ASTM E-8M, depicted in Figure 1, were manufactured and tested in both the L- and T-direction.

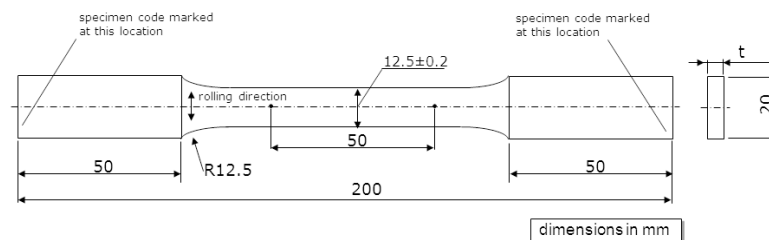


Figure 1: ASTM E-8M sheet-type static specimen

The static tensile tests are performed in accordance with test method ASTM E8/E8M-11 [3]. The tests are done in an INSTRON model 5882 testing machine with a maximum capacity of 100 kN, using INSTRON 5800 controller and software. An extensometer with 50 mm gauge length was calibrated for 2% strain. The specimen was loaded with a constant strain rate of 0.00025 +/- 0.0001 m/m/s based on the extensometer strain till 2% (determined with extensometer) and increased with a strain rate to maximal 0.0025 m/m/s based on the crosshead rate after 2%. The stress-strain curves are depicted in Figure 2 and the resulting average mechanical properties are presented in Table II. These values correlate well with other sources, e.g. [7].

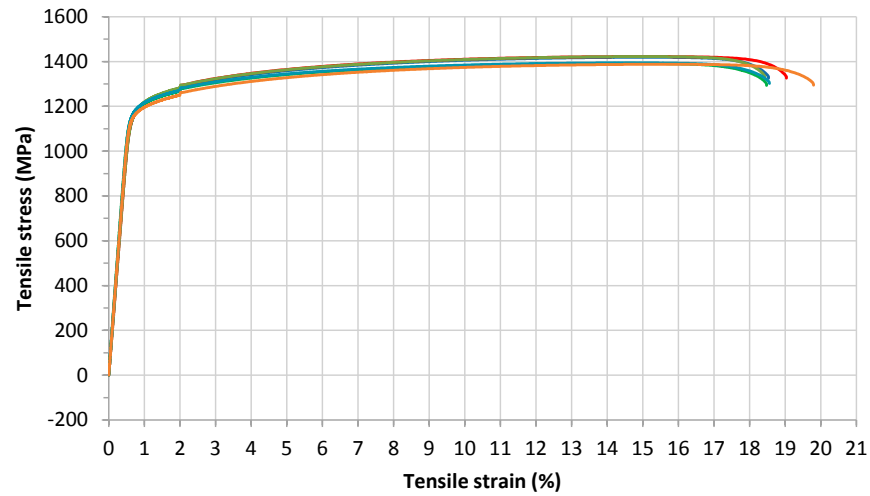


Figure 2: Measured stress-strain curves of the IN718 material

Direction	Ultimate tensile stress (MPa)	Tensile strain at break (%)	0.2% Yield stress (MPa)	Young's Modulus (GPa)
L	1420	18.6	1180	203
T	1390	19.0	1180	212

Table II: Average mechanical properties of the IN718 material

#### Fatigue crack growth tests

All fatigue crack growth tests were performed in a closed loop servo-hydraulic Wolpert-Amsler-2 testing machine with a maximum capacity of 200 kN, using an INSTRON controller and software. The specimens were clamped with hydraulic jaws with a straight gripping face (using the maximum available clamping surface maximising the clamping area) and accurately aligned in the clamping devices to guaranty a proper uniform tensile loading of the specimen minimising unwanted bending effects and slip of the specimen. Since no compression loads are present in the spectra, no anti-buckling guide was needed. All specimens are pre-cracked in accordance with ASTM E647 until a crack extension of approximately 0.3 mm was obtained using a CA load of  $R=0.1$  and maximum stress of 600 MPa for the SET and 400 MPa for the MT specimens. All specimens were cut in the rolling direction of the plate.

#### Moderate load fatigue crack growth test specimen

The moderate load fatigue crack growth tests were performed on MT specimens. The overall geometry is similar to that of the SET specimens (Figure 3). A hole of 0.8 mm diameter was

drilled in the middle of the specimen and a notch of 0.35 mm was introduced by EDM on both sides of the hole.

#### Large scale plasticity fatigue crack growth test specimen

The specimen for the large scale plasticity fatigue crack growth tests in Table I is a single edge crack tension (SET) specimen. Due to the high loads above the yield stress, this specimen was selected instead of the more common MT or compact tension (CT) specimen. Both specimen types would lead to unwanted deformations, for the MT specimen around the starter notch. For the same reason a uniform load is applied instead of the eccentrically-loaded SET specimen listed in ASTM E-647, preventing excessive deformations and/or early failure around the pin-holes. Furthermore, the starter notch is kept as small as possible. A second reason for this was the short crack growth life and a small critical crack length predicted by NASGRO in the design stage. Nevertheless, it was decided to first try a (small) through crack for which crack lengths can be monitored much easier than a small corner or surface crack. Downside of this specimen and loading condition is the possible secondary in-plane bending effect that can play a role at larger crack lengths. As explained later, the objective here was to look at small crack lengths (< 10 mm) only.

The geometry and dimensions of the selected SET specimen are depicted in Figure 3. The thickness of 3.2 mm was selected since it is a typical thickness used in various engine components. At the crack region the specimen is 40 mm wide and has straight edges over 50 mm, where the width is based on the capacity of the testing machine. A small curvature is added to ensure that plasticity occurs at the cracked region and to increase the width of the clamping area to prevent slip at the large loads. For the same reason, the height of the clamping area was selected the maximum depth of the clamping gripping face. A notch of 0.35 mm was introduced by electric discharge machining (EDM) over the whole thickness at one edge of the specimen.

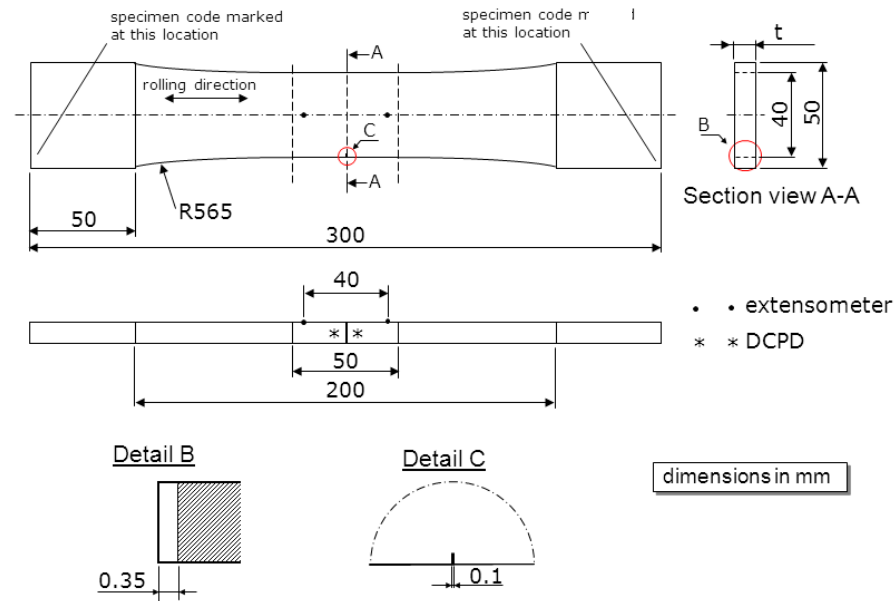


Figure 3: Single edge crack tension (SET) fatigue crack growth specimen

### Loads

All load spectra applied for the moderate load and large scale plasticity fatigue crack growth tests of Table I are depicted in Figure 4. The load controlled CA baseline spectra applied to the MT specimens, without (LS3a) and with large scale plasticity cycle (LS3b), consisted of a maximum stress of 800 MPa for R ratios: 0.2, 0.5, 0.65, and 0.8. The large scale plasticity pre-cycle up to 1.3% total strain in spectrum LS3b was applied before the notch was inserted in the specimen.

The large scale plasticity displacement controlled spectra (LS1 and LS2) include a large cycle up to 1% total strain after which CA or VA cycles are applied. The VA spectra consists of a repeated LCF cycle (representing the temperature profile during an engine start/stop) with a superimposed HCF random spectrum of 1000 cycles according to a Rayleigh distribution, with parameter value 0.0325 % strain, representing a typical dynamic load generated with ESALOAD. The HCF spectrum is repeated 5 times per LCF cycle.

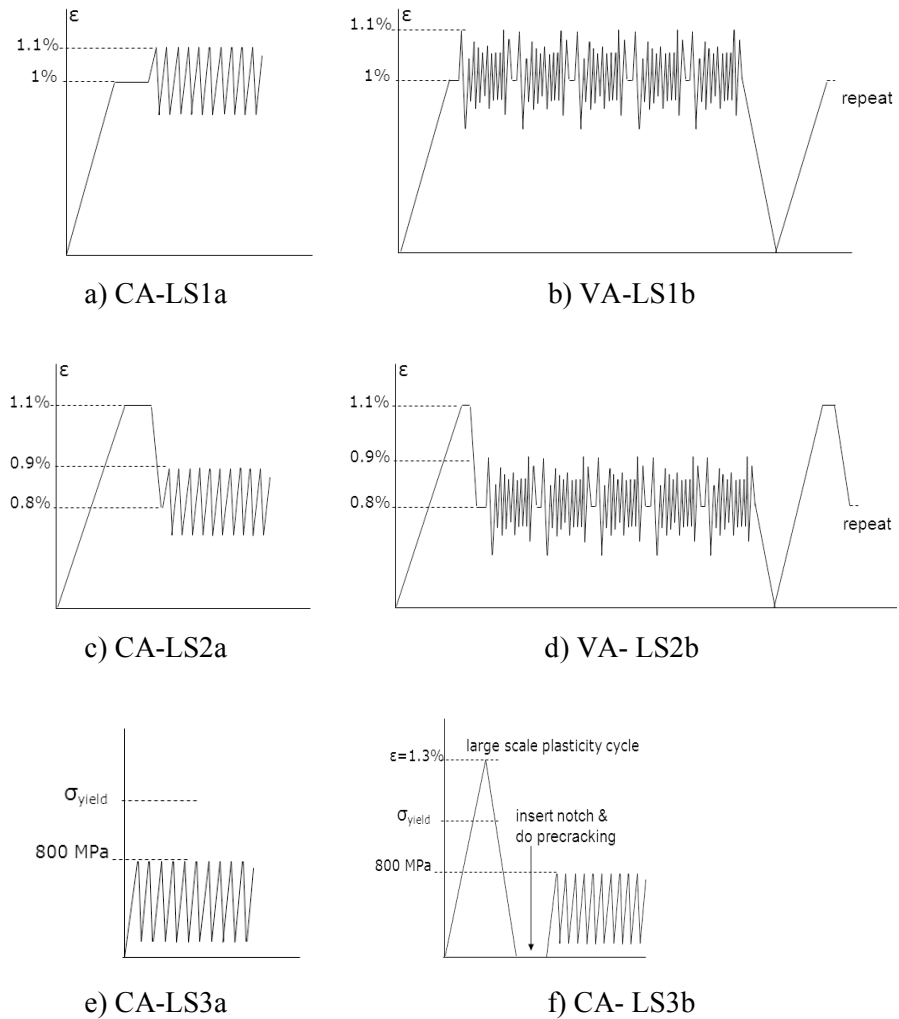


Figure 4: Schematic representation of the various load spectra

With the MT and SET CA tests the question can be answered whether LEFM (stress intensity factor solutions and corresponding crack growth equations) can still be applied for life prediction at these high load levels. With the SET VA tests the load interaction effects at these high load levels can be examined. The LCF cycle is repeated here as well to arrive at a more realistic design spectrum and to introduce additional load interaction effects.

It is not unlikely that in practice, the load decreases after plastically deforming the material due to decreasing thermal gradients, e.g. after engine start-up. For these reasons, the alternative spectrum LS2 was applied consisting of a large cycle (after pre-cracking) causing plasticity and then a constant amplitude sequence at a somewhat lower strain level to determine whether LEFM is applicable. Another reason to apply such a spectrum is the more pronounced retardation effects representing a kind of spike-load sequence.

### Test results

Displacement measurements were performed with a calibrated extensometer with 40 mm gauge length on the front side of the specimen located near the middle of the specimen at the opposite side of the crack. Crack length measurements were performed by means of two high-resolution photo cameras installed on the front and rear side of the specimen and by means of a Direct Current Potential Drop (DCPD) system. The requirement of a uniform current density at a cross section remote from the crack plane was met by introducing a current over the whole specimen ends. The length to width ratio of the specimen was  $100/40=2.5$ , which sufficed as well.

Figure 5 shows an example of the test results obtained for the various SET and MT specimens. The pictures consist of:

- Recorded strain data (SET specimens only)
- Recorded load data
- Recorded DCPD data
- Crack growth curve from DCPD and photos
- Crack growth rate versus  $\Delta K$  (CA only)
- Numerical versus experimental crack growth curve (CA only)

The first three pictures depict the measured data: strain, load and DCPD, the last three depict derived data. In picture a) the development in strain value can be observed, showing a straight line for the CA displacement load. The load level depicted in picture b) drops as the crack advances. Since the SET tests were performed under displacement control, the load decreases for increasing crack lengths due to the reduced stiffness of the specimen. As a result, the crack growth rate decreases for increasing crack lengths as well. Hence, most tests were ended after the crack grew outside the photographed region. Especially the variable amplitude tests became extremely slow due to the many small amplitude cycles and were stopped at a smaller crack length than the CA tests. Two CA specimens were continued close to breakage, showing hardly any crack growth, demonstrating the possibility of having a stable crack of large length even at these high load levels. The force level had dropped to less than 7 kN, while being 159 kN at the start of the test.

In all tests a reference MT or SET specimen with a notch only was used to compensate for temperature effects. The DCPD value exported by the system is the ratio of the voltage measured on the test and the reference specimen, depicted in picture c). The start DCPD value therefore lies close to 1. The DCPD system has a hardware limit of 9 volt, which is reached for the SET specimen for a crack length of approximately 7 mm, which sufficed for our purpose. Moreover, the photo cameras were positioned such that a crack of approximately 10 mm was



covered, to allow for accurate crack length measurements, see Figure 6. Therefore, crack growth data was gathered from an initial crack length of around 0.6 mm up to about 7 mm.

The MT specimens, having a larger notch, did not suffer from the 9 volt limit of the DCPD device. Also the cameras were installed to record the complete specimen width. For most of the MT specimens the DCPD values were unreliable for crack lengths below the 2 to 3 mm. The exact cause for this is not clear, but might be due to: a larger lead spacing distance of 4 mm than the 1 mm for the SET specimens; a different attachment of the wires, welded for SET and a pin in a hole for MT; or related to the lower maximum load level of 1230 MPa for SET and 800 MPa for MT yielding a smaller crack opening.

The crack growth curve in picture d) is determined from the DCPD data according to the analytical voltage versus crack size relation from ASTM E647-11 [5]:

$$a = \frac{2W}{\pi} \cos^{-1} \left( \frac{\cosh\left(\frac{\pi}{2W} y_0\right)}{\cosh\left(\frac{V}{V_r} \cosh^{-1}\left(\frac{\cosh\left(\frac{\pi}{2W} y_0\right)}{\cos\left(\frac{\pi}{2W} a_r\right)}\right)\right)} \right) \quad (1)$$

where:

$a$  = the crack size,

$a_r$  = the reference crack size (here obtained from a foto),

$W$  = the specimen width,

$V$  = the measured DCPD voltage,

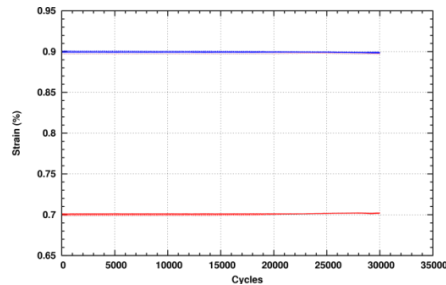
$V_r$  = the measured voltage corresponding to  $a_r$ , and

$y_0$  = the voltage measurement lead spacing from the crack plane.

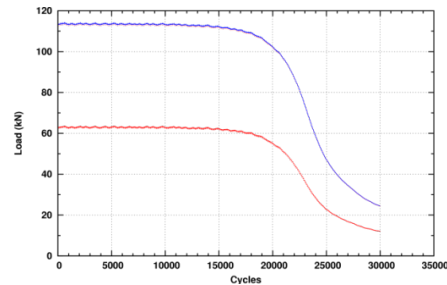
ASTM E647-11 only refers to the MT specimen in conjunction to the above formula, but reference [6] shows the applicability of the formula for CT and SET specimen as well. Moreover, it was demonstrated that the formula shows some deviation from the experimental data at larger crack lengths. Hence, a small crack length should be used as reference. On the other hand the measurement error for a small crack is larger. Therefore, the smallest crack length for which the length could be determined accurately was used as reference.

During the test photos were taken of the crack plane at regular intervals from the front and rear of the specimen, an example is shown in Figure 6. From these photos a number of average crack lengths were determined with corresponding cycle number and DCPD value, depicted by the

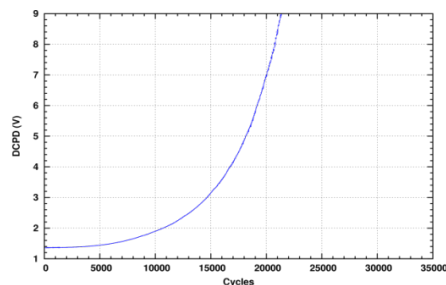
dots in picture d), to validate the DCPD data. One of these points was used in the above formula as reference crack length and corresponding reference voltage.



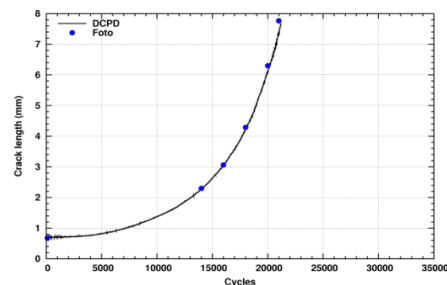
a) Recorded strain



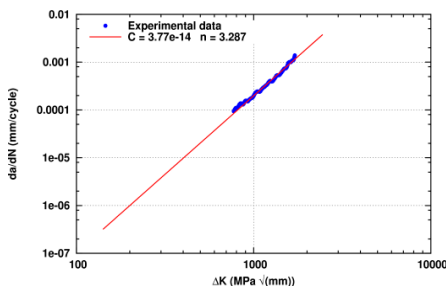
b) Recorded load



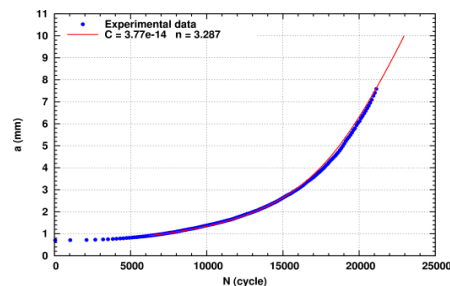
c) Recorded DCPD



d) Crack growth curve from DCPD and photos



e) Crack growth rate versus  $\Delta K$



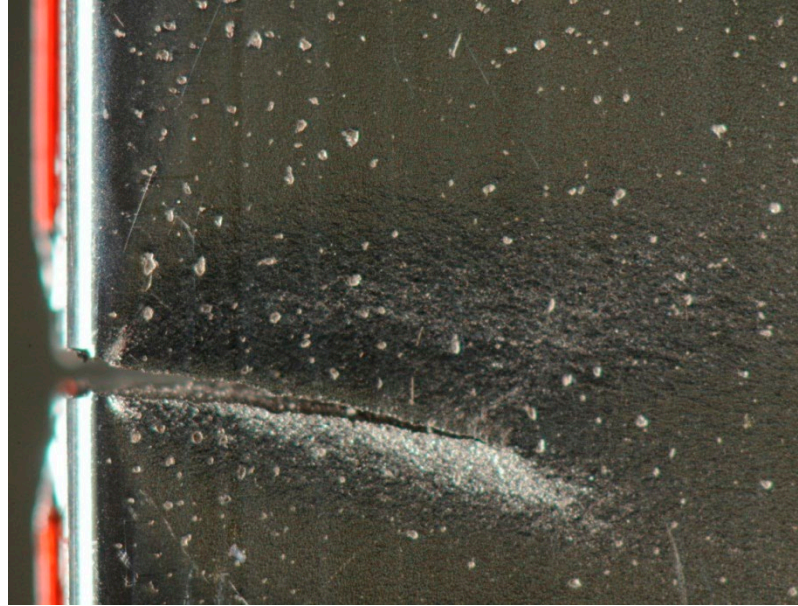
f) Numerical vs experimental crack growth

Figure 5: Test results for LS2a

The DCPD method generated a lot of data from which the crack growth curve was established. This data could not be used directly to determine the crack growth rate for the CA tests, due to some scatter in the DCPD data, somewhat higher for small crack lengths. Hence, to reduce the scatter an average crack length was determined over 100 cycles and a minimum crack advance of 0.01 mm. The resulting smoothed data values are represented as dots in pictures e) and f). From this crack growth data the crack growth rate, depicted in picture e), is determined according to the procedure described in ASTM 647-11 using an incremental polynomial method fitting a second-order polynomial to sets of 9 successive data points. Next, this crack growth rate data is used in a least-square fit of the Paris crack growth equation, also depicted as a drawn

line in picture e). Subsequently, this fit is used to simulate the experimental crack growth curve to check for a proper fit, depicted as a drawn line in picture f).

Figure 9 depicts the final crack growth rate data as function of  $\Delta K_{eff}$  for both the SET and MT specimens, correcting for the difference in R-values using the Schijve opening function.



*Figure 6: Example photo of the front of the crack front taken during the fatigue test to monitor the crack length*

It was observed that slanted crack growth (single or double shear) occurred for the large scale plasticity SET specimens loaded by the CA spectra (LS1a and LS2a in Table I), while the specimens loaded by the VA spectra (LS1b and LS2b) showed square (flat) crack growth, depicted in Figure 7. An explanation of this phenomenon is given below.

The MT specimens showed slanted crack growth as well for R equal to 0.2, 0.5, 0.65. For R equal to 0.8 squared crack growth was obtained, as depicted in Figure 8. According to ASTM E647-11, the MT specimen remains predominantly elastic at all values of the applied force since:

$$W - 2a \geq 1.25 \frac{P_{max}}{t \sigma_{yld}} \quad (2)$$

The maximum applied force  $P_{max}$  during the test equalled 102.9 kN. With a specimen width  $W$  of 40 mm, a thickness  $t$  of 3.2 mm and a 0.2% yield stress  $\sigma_{yld}$  of 1180 MPa, the maximum allowable crack size  $2a$  equals 12.7 mm.

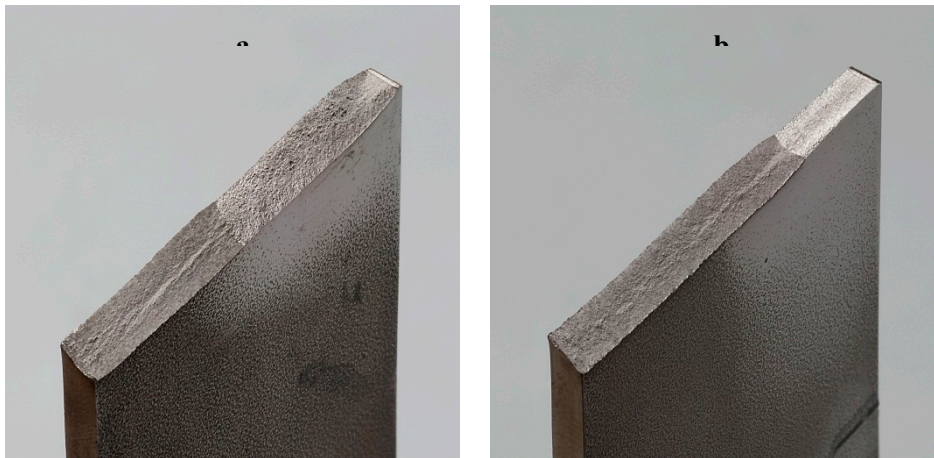


*Figure 7: Fracture surface of CA (a) and VA (b) loaded SET specimen, from right to left showing the notch, the pre-crack, the slanted (a) and square (flat) (b) fatigue crack and the final rupture surface*

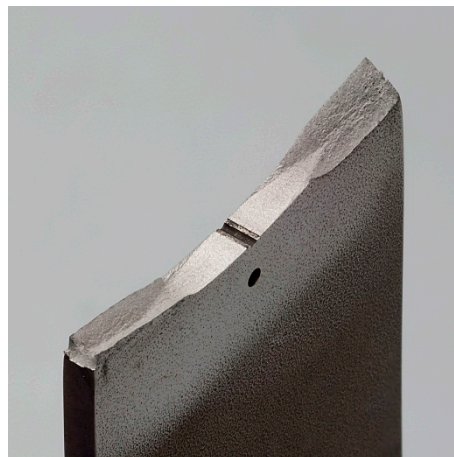


*Figure 8: Fracture surface of CA loaded (R=0.8) MT specimen, from inward showing the notch, the pre-crack (hard to see in the picture), the square (flat) fatigue crack and the final (slanted) rupture surface.*

### 3 Analysis

#### Moderate load fatigue crack growth

Fatigue crack growth rate versus effective stress intensity factor range for the load controlled CA tests on the MT specimens is depicted in Figure 9. The tests without initial plastic deformation are denoted with 'normal' and have a closed symbol, whereas the test for the same R-ratio with plastic deformation is denoted as 'plastic' and has the same symbol in an open variant. The effective stress intensity factor was determined using the empirical equation by Schijve [8]:

$$\Delta K_{eff} = (0.55 + 0.33R + 0.12R^2)\Delta K \quad (3)$$

In which  $\Delta K_{eff}$  is the effective stress intensity factor range,  $R$  is the stress intensity factor ratio and  $\Delta K$  is the stress intensity factor range. The figure shows that there is no significant influence of plastic pre-deformation on the fatigue crack growth rate. It also shows that the Schijve correlation in equation (3) collapses data for different R-ratios on one line indicating Paris like behaviour.

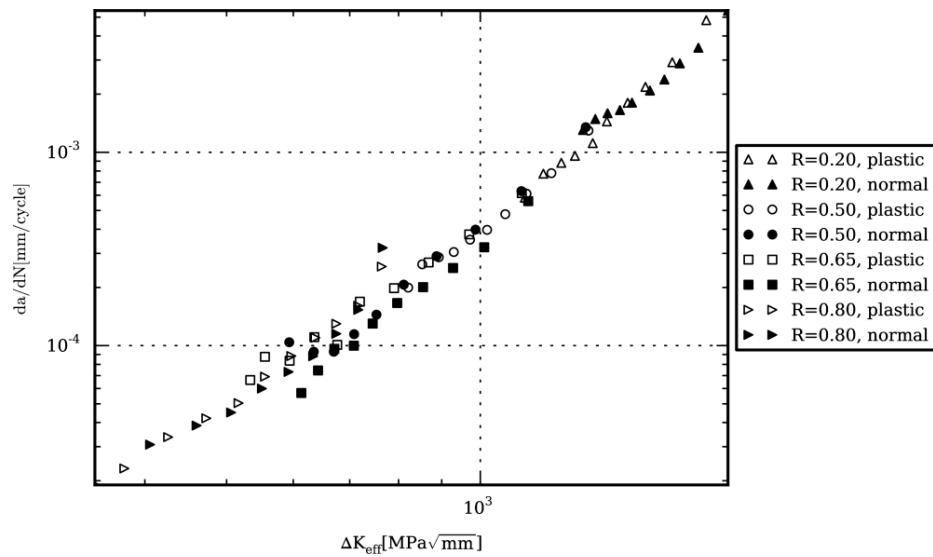


Figure 9: Fatigue crack growth rate versus  $\Delta K_{eff}$  for the CA loaded MT specimens

Figure 10 again shows the data from the tests. Only the data without plastic pre-deformation are included for clarity (again in closed symbols). It also shows the fatigue crack growth rates determined using the NASGRO equation with the data contained in the NASGRO software, denoted as NASGRO and depicted using corresponding open symbols. Additionally, the figure contains the measured fatigue crack growth rates used to determine the constants in the

NASGRO equation (labelled as 'data'). The predictions were made for the 20°C fit. The figure shows that the NASGRO predictions are in the stable tearing crack growth region near the fracture toughness with growth rates increasing above the Paris line. The  $R=0.8$  test data on which the NASGRO database constants (extracted from the NASGRO database) are based confirms this behaviour. However, the data from the current tests stay on the Paris line. The test data from the NASGRO database at other  $R$  ratios leads to the same conclusion.

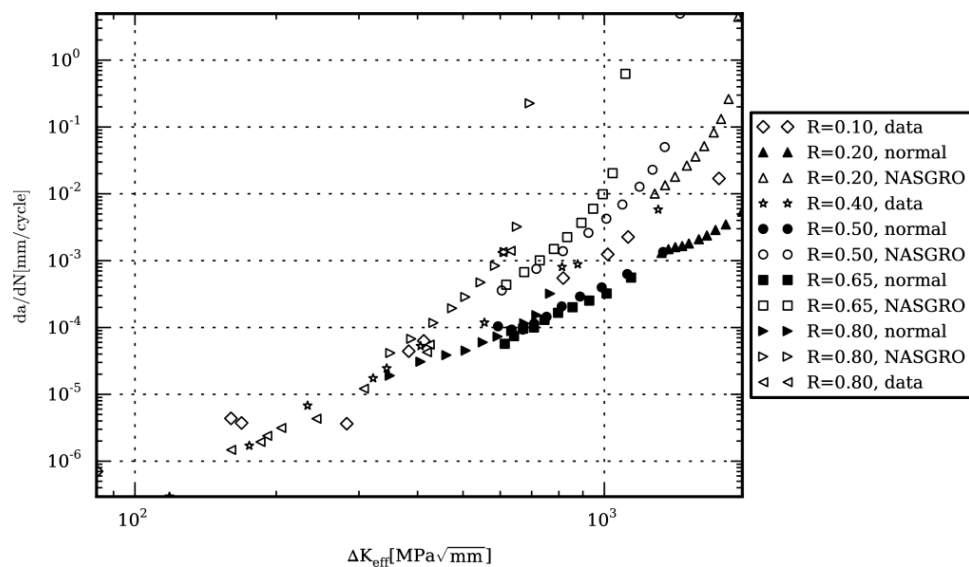


Figure 10: Comparison of current fatigue crack growth rates with NASGRO reference data

#### Constant amplitude large scale plasticity fatigue crack growth

Fatigue crack growth tests were performed on SET specimens at loads close to the yield limit. Two  $R$ -ratios were used and two specimens were tested for each  $R$ -ratio. The resulting fatigue crack growth rates are shown in Figure 11 together with the growth rates for the moderately loaded specimens without plastic pre-deformation discussed previously. The figure also shows a Paris law fit with factor 2 scatter bands. The figure shows that the growth rates for high loads are very similar to those for the more moderate loads and they show a Paris region over large portions of the test. The data at high loads do show first signs of a stable-tearing crack growth region, with growth rates increasing above the line representing Paris behaviour.

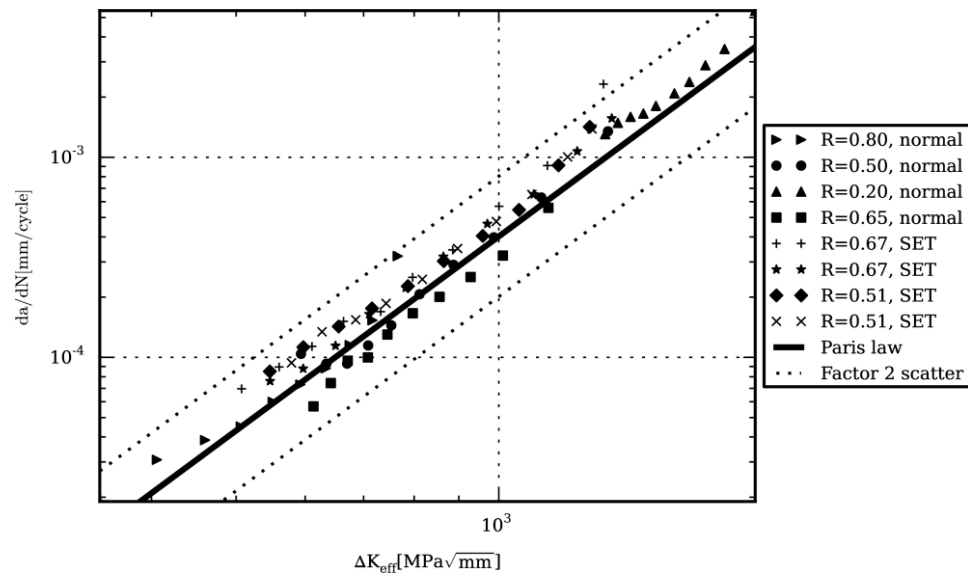


Figure 11: Comparison of the moderate load and high load constant amplitude fatigue crack growth

#### Variable amplitude large scale plasticity fatigue crack growth

Figure 10 showed that fatigue crack growth rates predicted using the data in the NASGRO material database are much higher than those determined in the current tests. It is therefore unlikely that variable amplitude tests can be accurately predicted using these data. The Paris behaviour depicted in Figure 11 is therefore used for variable amplitude life prediction. A TC14 displacement controlled geometry with a length of 40 mm (equal to the opening of the strain gauge) is used with type I boundary conditions and under plane stress conditions. The applied displacement is corrected for the plastic deformation because TC14 assumes linear elasticity. Figure 12 shows the measured and predicted fatigue crack growth curves for the high mean and the reduced mean spectrum. Only one of the two identical tests is shown to improve clarity, because both tests yielded highly similar results. Predictions using the Paris behaviour are denoted as 'Paris'. The measured crack growth life (closed symbols) is similar to the predicted crack growth, but the measured crack growth rate is lower for small crack length and higher for longer cracks. The Generalized Willenborg (GW) model was applied as implemented in the NASGRO software to implement retardation effects using a Shutoff Overload Ratio (SOR) of 3.0. The crack growth curves are also included in Figure 12 (denoted as Paris, GW) and are almost identical to the non-interaction results. The reason is that the spectrum consists of small  $\Delta K$  cycles on a large  $K_{max}$  value. The plastic zone size for all these cycles, related to  $K_{max}$  is similar and therefore very little retardation will be predicted by the Willenborg model.

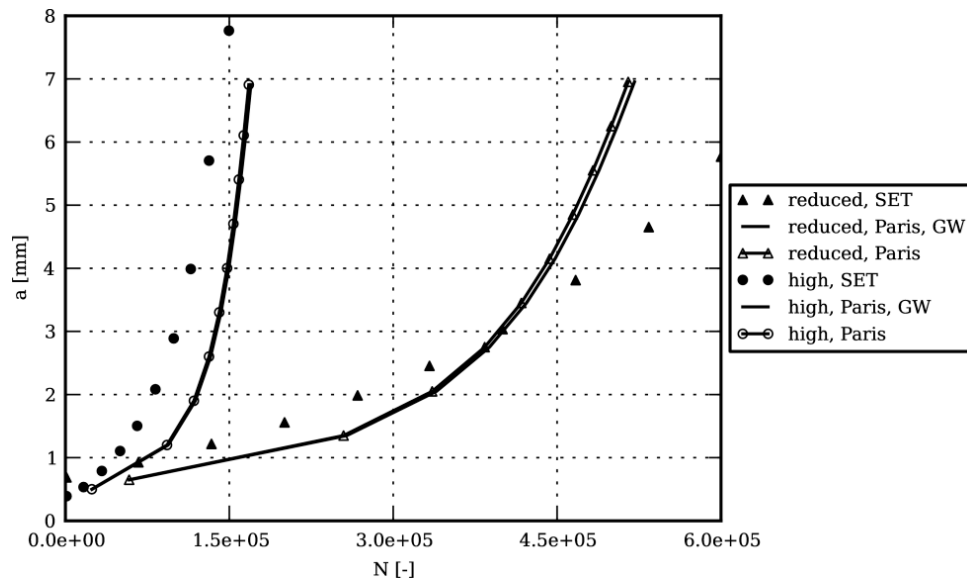


Figure 12: Predicted and measured variable amplitude crack growth for high loads

A notable new perception of variable amplitude crack growth is pioneered by DSTO [9]. They propagate exponential crack growth leading to a log-linear relation between crack length and number of cycles, as depicted in Figure 13. The figure shows that the high mean data show a very accurate log-linear behaviour, whereas the reduced mean data also shows good correspondence with log-linear behaviour. The same plot is shown in Figure 14 for the constant amplitude data. These data do not match with the log-linear behaviour as the variable amplitude data does for two reasons. Firstly, the CA data deviate more from the log-linear line than the VA data. Secondly, the VA data form a straight or slightly convex curve where the CA data forms a concave curve. It is unlikely that a retardation model will transform the concave CA curve into the straight VA curve. This is also clear from both the CA and VA predictions in the plot. They all show the CA concave behaviour. The exponential crack growth observation for VA spectra does not yield an easy crack growth prediction method though, because the parameters for the fits depend on the spectrum. This is clear in the figure, the fit for the high mean spectrum has a different slope as the fit for the reduced mean spectrum and they will also be different when other characteristics of the spectrum change.

A further problem would be that the constant amplitude crack surface is slanted, whereas the variable amplitude surface is square (flat) (Figure 7). The reason is likely that the VA spectrum contains many small cycles with corresponding small crack growth rates. Square (flat) crack growth is then favoured over slant crack growth. The few large cycles are then unable to enforce slant crack growth. A third observation is that the variable crack surface is smoother than the constant amplitude surface, which can be clearly observed in Figure 7.



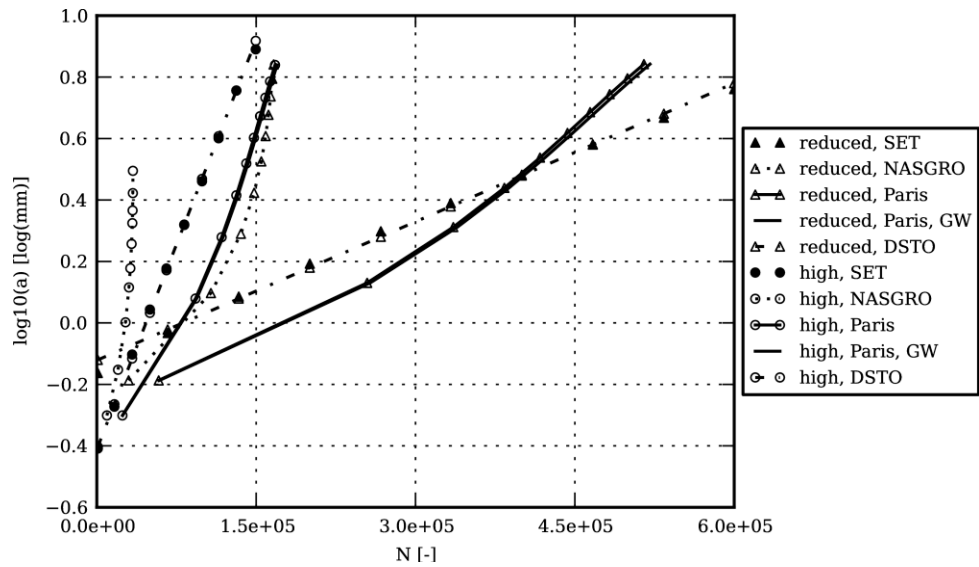


Figure 13: Log-linear relation between crack length and number of cycles for the VA tests

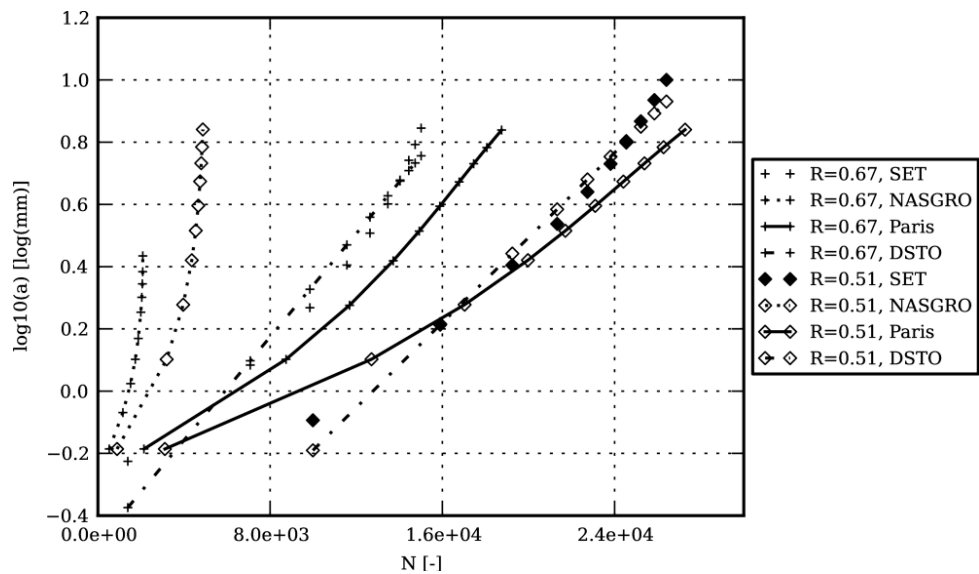


Figure 14: Log-linear relation between crack length and number of cycles for the CA tests

### Frequency influence

Two tests were performed at significantly lower frequencies than all other tests. The constant amplitude tests for  $R=0.685$  was nominally performed at 1 Hz but was also performed once at a frequency of 0.25 Hz. The result depicted in Figure 15 show a markedly higher fatigue crack growth rate for the lower testing frequency. A second test at different frequency was a variable amplitude test at 0.5 Hz as opposed to the normal test frequency of 2 Hz. The results shown in Figure 16 again suggest a significantly higher crack growth rate at lower frequency. The crack

surfaces show much more dimples for the lower frequency tests, indicating that the stable tearing crack growth [8] becomes more important. Frequency dependent crack growth rates are often observed in IN718 at elevated temperatures and attributed to oxidation or corrosion [10], but the tests in this work were performed at ambient conditions. The reason for this apparent frequency influence is currently unclear.

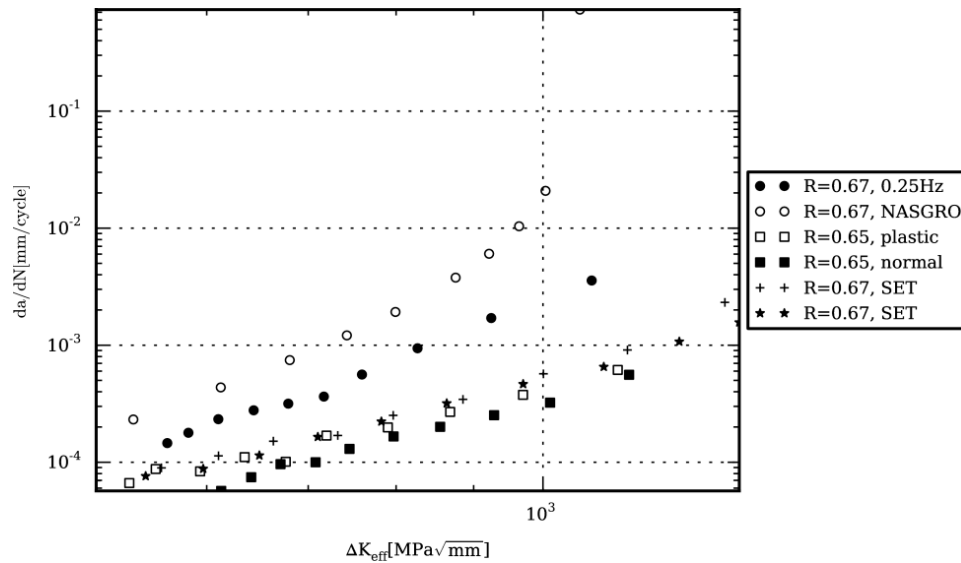


Figure 15: Frequency influence under CA loading

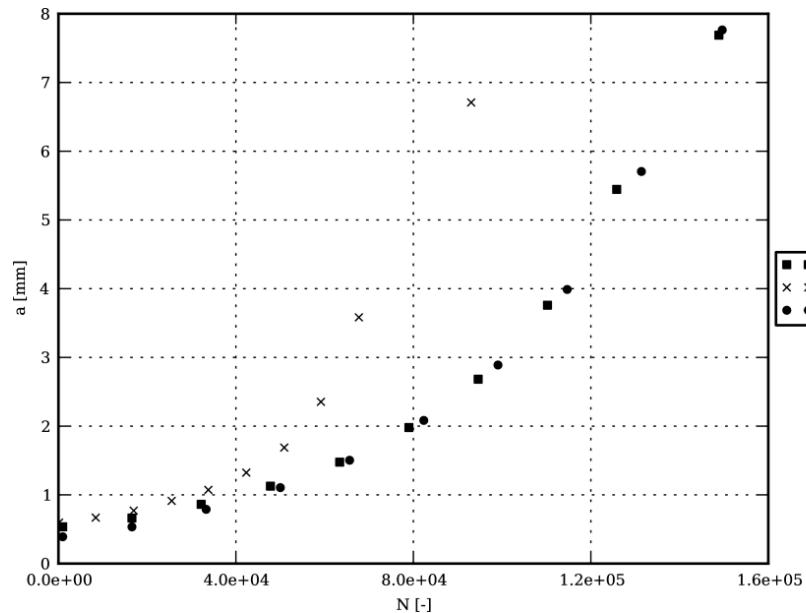


Figure 16: Frequency influence under VA loading

## 4 Conclusions

- No influence of plastic pre-deformation on fatigue crack growth was observed (Figure 9).
- Fatigue crack growth rates measured under high loads show Paris like behaviour up to failure. The fatigue crack growth rates are significantly lower than those in the NASGRO database. Furthermore, the typical increasing crack growth rates towards the critical stress intensity factor are not clearly present. Although the material constants are different from those found in the NASGRO database, LEFM can still be applied using stress intensity factors and a crack propagation law. The highly loaded SET specimens show similar behaviour as the MT specimens under lower applied stresses.
- Variable amplitude crack growth is significantly slower than predicted using a non-interaction model based on the observed Paris like behaviour. Adding a generalized Willenborg retardation model has little influence due to the high R-ratio of the load spectrum and is therefore not useful.
- There seems to be a substantial influence of frequency on growth rates notwithstanding that the tests were performed at ambient conditions. The growth rates increase at lower test frequencies.

## ACKNOWLEDGEMENT

The research presented was funded by the European Space Agency ESA under contract 4000102474/11/NL/RA.

## References

- [1] NASGRO, Fracture Mechanics and Fatigue Crack Growth Analysis Software, <http://www.nasgro.com/>.
- [2] Anon; Aerospace series Heat resisting alloy NI-PH2601 (NiCr19Fe19Nb5Mo3) Solution treated and precipitation treated Sheet, strip and plate  $0.2 \text{ mm} \leq a \leq 10 \text{ mm}$ , prEN2407 Edito P 1, *AECMA Standard*, December 1998.
- [3] Anon; Standard Test Method for Tension Testing of Metallic Materials, ASTM E8/E8M-11, *American Society for Testing and Materials*, December 2011.
- [4] Veul, R.P.G., Brunetti, F., Sinnema, G., Henriksen, T.K.; *ESALOAD User's manual, version 4.2.2*, Annex 1 of ESACRACK Manual TEC-MCS/2006/1448/In/GS Issue 4, March 2012. <http://www.esacrack.com>
- [5] Anon; Standard Test Method for Measurement of Fatigue Crack Growth Rates, ASTM E647-11e1, *American Society for Testing and Materials*, June 2011.
- [6] Schwalbe, K. -H. and Hellmann, D.; Application of the Electrical Potential Method to Crack Length Measurements Using Johnson's Formula, *American Society for Testing and Materials*, pp. 218-220, 1981.
- [7] Rice, R.C; Jackson, J.L., Bakuckas, J. and Thompson, S.; *Metallic Materials Properties Development and Standardization (MMPDS)*, DOT/FAA/AR-MMPDS-01, 2003.
- [8] Schijve, J. (2009), *Fatigue of Structures and Materials*, Springer, Houten.
- [9] Molent, L.; McDonald, M.; Barter S. and Jones R., Evaluation of spectrum fatigue crack growth using variable amplitude data, *International Journal of Fatigue* 30, pp. 119-137, 2008.
- [10] Chan, K.S.; Enright, M.P.; Moody, J.P.; Hocking, B. and Fitch, S.H.K., Life prediction for turbopropulsion systems under dwell fatigue conditions, *Journal of Engineering for Gas Turbines and Power*, vol. 134, 2012.